J|A|C|S ARTICLES

Published on Web 05/13/2009

Effects of Weak Intermolecular Interactions on the Molecular Isomerism of Tricobalt Metal Chains

Rasmus D. Poulsen,[†] Jacob Overgaard,[†] Alexander Schulman,[‡] Christina Østergaard,[†] Carlos A. Murillo,[§] Mark A. Spackman,[⊥] and Bo B. Iversen*[,†]

Department of Chemistry, University of Aarhus, DK-8000 Aarhus, Denmark, Department of Applied Surface Chemistry, Chalmers University, S-412 96 Gøteborg, Sweden, Department of Chemistry, Texas A&M University, PO Box 30012, College Station, Texas 77842-3012, and School of Biomedical, Biomolecular and Chemical Sciences, University of Western Australia, Crawley, Western Australia 6009, Australia

Received November 20, 2008; E-mail: bo@chem.au.dk

Abstract: Depending on the number of interstitial solvent molecules, *n*, crystals of the linear chain compound Co_3(dipyridylamide)$_4Cl_2 \cdot n CH_2Cl_2$ adopt either symmetrical or unsymmetrical metal chain structures. We explore here the possible reasons for such behavior using Hirshfeld surface analysis of intermolecular interactions as well as the charge density determined from 100(1) K X-ray diffraction data on the unsymmetrical complex Co_3(dipyridylamide)$_4Cl_2 \cdot 2.11CH_2Cl_2$, *u*-**1**, and crystal structures of *u*-**1** determined from single crystal synchrotron X-ray diffraction data at 20, 150, and 300 K. The new crystal structures are compared with previous structural results on a crystal with slightly different solvent content. This change in solvent content only affects the bond distances to atom Co(3), which are also strongly affected by temperature changes due to a spin crossover transition. Large differences in intermolecular interactions are revealed by the Hirshfeld surface analysis between symmetrical (*s*-**1**) and unsymmetrical (*u*-**1**) crystal solvates, suggesting that the molecular isomerism is strongly influenced by crystal packing effects. Topological analysis of the static electron density of *u*-**1** suggests that there is direct metal−metal bonding for both the shorter Co(1)−Co(2) and the longer Co(2)−Co(3) contact. The approximate description of the system as a $(Co_2)^{2+}$-dimer and an isolated Co^{2+}-ion is reflected in the character of the metal−ligand interactions, which are more ionic for the isolated Co(3) atom, and the topological charges $Co(1)^{+0.50}$, $Co(2)^{+0.77}$, and $Co(3)^{+1.36}$. The two termini of *u*-**1** are found to be very different, both in terms of structural surroundings as well as topology. The central Co(2) atom is similar to a cobalt atom in a tetragonally distorted octahedral environment resulting in preferred occupancy in the t_{2g} orbitals. The Co(1) atom has significant deformation in the *xz* and *yz* planes (*z* along the chain axis, *x* and *y* toward ligands) reflecting covalent interactions with the terminal chlorine atom Cl(1). The Co(3) atom has a relatively high occupancy of the $d_{x^2-y^2}$ orbital and a relatively low occupancy of the d_{xy} orbital confirming that these orbitals are involved in the spin crossover process and predominantly responsible for the observed variation in bond lengths with temperature.

Introduction

Polynuclear transition metal complexes are of great importance across many scientific disciplines.[1] The electronic structure of such species presents a considerable challenge to *ab initio* theoretical methods, and this makes the field a fertile meeting ground for experiment and theory.[2] Strong interest has centered on polynuclear species with shallow potential energy surfaces (PES), where subtle changes in thermodynamical parameters or the surroundings of the system (crystal or supramolecular effects) can lead to dramatic changes in the structure and properties of the complex.[3] Examples are mixed valence trinuclear basic carboxylates ($[M^{III}_2M^{II}O(O_2CR)_6L_3] \cdot nS$),[4] and Cu complexes exhibiting dynamic Jahn−Teller distortions.[5] The former provide good model systems for the active sites of enzymes, and allow detailed studies of electron transfer processes. In the trinuclear basic carboxylates subtle changes

[†] University of Aarhus.
[‡] Chalmers University.
[§] Texas A&M University.
[⊥] University of Western Australia.

(1) Lippard, S. J. *Angew. Chem.* **1998**, *100*, 353−370; *Angew. Chem., Int. Ed. Engl.* **1988**, *27*, 344−361.
(2) Rohmer, M. M.; Benard, M. *Chem. Soc. Rev.* **2001**, *30*, 340–354.
(3) (a) Cotton, F. A.; Herrero, S.; Jiménez-Aparicio, R.; Murillo, C. A.; Urbanos, F. A.; Villagrán, D.; Wang, X. *J. Am. Chem. Soc.* **2007**, *129*, 12666–12667. (b) Cannon, R. D.; White, R. P. *Prog. Inorg. Chem.* **1988**, *36*, 195–297. (c) Oh, S. M.; Hendrickson, D. N.; Hassett, K. L.; Davis, R. E. *J. Am. Chem. Soc.* **1985**, *107*, 8009–8018. (d) Ammeter, J. H.; Bürgi, H. B.; Gamp, E.; Meyer-Sandrin, V.; Jensen, W. P. *Inorg. Chem.* **1979**, *18*, 733–750.
(4) (a) Dziobkowski, C. T.; Wrobleski, J. T.; Brown, D. B. *Inorg. Chem.* **1981**, *20*, 679–684. (b) Woehler, S. E.; Wittebort, R. J.; Oh, S. E.; Hendrickson, D. N.; Inniss, D.; Strouse, C. E. *J. Am. Chem. Soc.* **1986**, *108*, 2938–2946. (c) Sato, T.; Ambe, F.; Endo, K.; Katada, M.; Maeda, H.; Nakamoto, T.; Sano, H. *J. Am. Chem. Soc.* **1996**, *118*, 3450–3458. (d) Overgaard, J.; Larsen, F. K.; Schiøtt, B.; Iversen, B. B. *J. Am. Chem. Soc.* **2003**, *125*, 11088–11099. (e) Wu, G; Zhang, Y.; Ribaud, L.; Coppens, P.; Wilson, C.; Iversen, B. B.; Larsen, F. K. *Inorg. Chem.* **1998**, *37*, 6078–6083.

 10.1021/ja8091032 CCC: $40.75

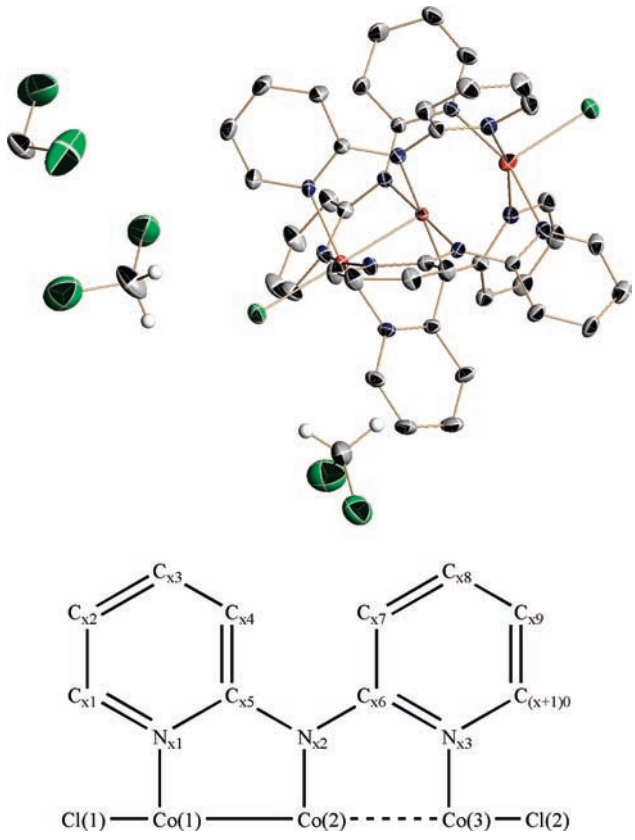

Figure 1. *u*-**1** molecule with three interstitial dichloromethane molecules at 100 K. The schematic shows the coordination environment of the metal centers and the nomenclature of the atoms. The four DPA fragments are labeled $x = 0$, 1, 2, and 3. Hydrogen atoms are removed for clarity. Atomic displacement ellipsoids are drawn at the 50% probability level.

in the crystal environment can suppress electron transfer processes and have significant effects on the molecular structure.[6] In dynamic Jahn−Teller complexes the crystal structure is strongly affected e.g. by H/D isotope substitution, which changes the unique axis of the Jahn−Teller distortion.[5] Another type of polynuclear species that often show dramatic structural behavior is the extended metal atom chain compounds[7] such as the trinuclear linear metal chain complex shown in Figure 1. For example, the title compound, $Co_3(dpa)_4Cl_2$, **1**, can be synthesized having either a symmetrical or unsymmetrical "Co_3" unit depending on small changes in the crystal environment. When crystallized with one CH_2Cl_2 solvent molecule, the symmetrical form (*s*-**1**) was obtained, while approximately 2.3 CH_2Cl_2 solvent molecules gave an unsymmetrical form (*u*-**1**) with $\Delta_{Co-Co} = 0.08$ Å and 0.17 Å at 20 and 298 K, respectively.[8] Thus, in this case inclusion of additional interstitial molecules has large consequences for the molecular structure. During the past decade a wide range of studies on linear chain metal complexes has been carried out.[9] These studies have shown that the two types of molecular isomers of **1** (i.e., *s*-**1** and *u*-**1**) are only observed in the solid state.[10] Thus, in solution only a single isomer is present (*s*-**1**), and this suggests that formation of isomerism is not due to an intrinsic molecular property but is determined by the crystal environment.

The $Cr_3(dpa)_4XY\cdot S$ system (X and Y are axial ligands, S is interstitial solvent molecule) also exists in both symmetrical and unsymmetrical forms.[11] It was suggested on the basis of a large number of crystal structures that strongly donating ligands favor a symmetrical structure (e.g., $X = Y = CN^-$, $S = CH_2Cl_2$), whereas weaker ligands (e.g., $X = Y = Cl^-$) favor the unsymmetrical structure.[11] Thus, in these studies of $Cr_3(L)_4XY\cdot S$ systems the molecular isomerism was considered a molecular effect with intrinsic competition in stability between an *s*-form and a *u*-form. From theoretical calculations on both the $Co_3(L)_4XY$ and $Cr_3(L)_4XY$ systems (i.e., gas phase without solvent) the *s*-form has been reported to be the ground state and no minima corresponding to the *u*-form were found.[12] However, because the actual molecular structures are experimentally determined in the crystalline phase by X-ray diffraction on specimens containing solvent molecules, direct comparison of these data is not possible. For the molecular isomerism in the title system $Co_3(dpa)_4Cl_2\cdot S$ there is also a remarkable magnetic behavior.[8] At low temperature *u*-**1** has an effective magnetic moment of ~2.9 μ_B, which increases to ~4.5 μ_B at 350 K. The corresponding values for *s*-**1** are ~2 μ_B and ~4 μ_B.

The electronic structure of the linear chain molecules is of fundamental interest for chemical bonding theory. For the $M_3(dpa)_4XY$ systems, three possible explanations for the molecular isomerism were advanced on the basis of DFT gas-phase theoretical analysis.[12] (i) Bond stretch isomerism with the existence of a double minimum on the PES, (ii) a shallow PES which can be perturbed by small external changes (e.g., crystal environment), and (iii) spin crossover, where the population of an unsymmetrical high-spin state increases with temperature. In case (iii) the specific temperature-dependent magnetic behavior of the $Co_3(dpa)_4Cl_2$ entity becomes intertwined with the molecular isomerism issue. The bond stretch isomer postulate (i) was ruled out since a single minimum corresponding to the *s*-form was obtained on the PES. It should be noted that *strictly speaking* the *u*-**1** and *s*-**1** systems can not be true bond isomers because they do not have identical crystal environments and differ in the number of interstitial molecules. With regard to (ii) simulations of a perturbed crystal environment in the form of point charges at opposite ends of the metal chain were not

(5) (a) Hathawat, B. J. *Coord. Chem. Rev.* **1981**, *35*, 211–252. (b) Simmons, C. J.; Hathaway, B. J.; Amornjarusiri, K.; Santarsiero, B. D.; Clearfield, A. *J. Am. Chem. Soc.* **1987**, *109*, 1947–1958. (c) Simmons, C. J. *New J. Chem.* **1993**, *17*, 77–95. (d) Iversen, B. B.; Larsen, F. K.; Figgis, B. N.; Reynolds, P. A. *Acta Chem. Scand.* **1994**, *50*, 800–809. (e) Figgis, B. N.; Iversen, B. B.; Larsen, F. K.; Reynolds, P. A. *Acta Crystallogr., Sect. B* **1993**, *49*, 794–806.

(6) (a) Kambara, T.; Hendrickson, D. N.; Sorai, M.; Oh, S. M. *J. Chem. Phys.* **1986**, *85*, 2895–2909. (b) Cannon, R. D.; Montri, L.; Brown, D. B.; Marshall, K. M.; Elliott, C. M. *J. Am. Chem. Soc.* **1984**, *106*, 2591–2594.

(7) See for example,(a) Berry, J. F. In *Multiple Bonds Between Metal Atoms*; Cotton, F. A., Murillo, C. A., Walton, R. A., Eds.; Springer Science and Business Media, Inc.: New York, 2005; pp 669−706 and references therein.

(8) Clerac, R.; Cotton, F. A.; Daniels, L. M.; Dunbar, K. R.; Kirschbaum, K.; Murillo, C. A.; Pinkerton, A. A.; Schultz, A. J.; Wang, X. P. *J. Am. Chem. Soc.* **2000**, *122*, 6226–6236.

(9) See e.g.: (a) Cotton, F. A.; Daniels, L. M.; Jordan, G. T.; Murillo, C. A. *J. Am. Chem. Soc.* **1997**, *119*, 10377–10381. (b) Clerac, R.; Cotton, F. A.; Dunbar, K. R.; Lu, T.; Murillo, C. A.; Wang, X. *J. Am. Chem. Soc.* **2000**, *122*, 2272–2278. (c) Clerac, R.; Cotton, F. A.; Daniel, L. M.; Dunbar, K. R.; Murillo, C. A.; Wang, X. *Inorg. Chem.* **2001**, *40*, 1256–1264.

(10) (a) Clerac, R.; Cotton, F. A.; Jeffrey, S. P.; Murillo, C. A.; Wang, X. *Inorg. Chem.* **2001**, *40*, 1265–1270. (b) Cotton, F. A.; Murillo, C. A.; Wang, X. *Inorg. Chem.* **1999**, *38*, 6294–6297.

(11) Berry, J. F.; Cotton, F. A.; Lu, T. B.; Murillo, C. A.; Roberts, B. K.; Wang, X. P. *J. Am. Chem. Soc.* **2004**, *126*, 7082–7096.

(12) (a) Benbellat, N.; Rohmer, M. M.; Benard, M. *Chem. Commun.* **2001**, 2368–2369. (b) Rohmer, M. M.; Benard, M. *J. Am. Chem. Soc.* **1998**, *120*, 9372–9373. (c) Rohmer, M. M.; Strich, A.; Benard, M.; Malrieu, J. P. *J. Am. Chem. Soc.* **2001**, *123*, 9126–9134.

able to enforce a change from the ground state *s*-**1** to a higher energy *u*-**1**. However, such simplistic modeling of crystal effects may not capture the essence of the very complex crystal environment. Since the molecular isomerism is a solid-state effect, a more rigorous theoretical analysis of the intermolecular interactions would be useful. The gas-phase theoretical analysis pointed in favor of the spin crossover explanation for the isomerism (iii), i.e., that an unsymmetrical high-spin excited state is thermally accessed from a symmetrical low-spin ground state. This can explain the persistence of *u*-**1** at low temperatures as well as the large temperature-dependent structural variations.[8] In order to explain why *s*-**1** also has a large change in magnetization with temperature, the study invoked a different excited state with a symmetrical structure to be accessible for the *s*-form. Pantazis and McGrady recently reported expanded gas-phase molecular calculations and found that *s*-**1** and *u*-**1** each have unique doublet ground-state structures and that the bond length changes could be explained by spin crossover populating quartet excited states.[13] It was noted that the variable bond length with temperature is related to a variable population in the $d_{x^2-y^2}$ orbital on the isolated Co(3) atom. However, since the gas-phase DFT calculations do not account for the crystal environment, it is still not clear how closely related the molecular isomerism is to the magnetization behavior of $(Co_3(dpa)_4Cl_2 \cdot S)$.

Much of the discussion about the chemical bonding in linear metal chain molecules has concerned the nature of the metal−metal bonding, i.e. delocalized three center three electron σ-bond over the three metal species in the *s*-form, versus localized bonding with a M_2^{2+} dimer and an isolated M^{2+} species in the *u*-form.[12,13] The bonding analysis in all cases has been formulated based on qualitative molecular orbital (MO) models, which may not capture all essential bonding features. In this report the $M_3(dpa)_4XY \cdot S$ systems are examined with more rigorous chemical bonding models such as the quantum theory of atoms in molecules (QTAIM), which is based on an experimental observable, the electron density (ED),[14] and which has been successfully applied e.g. to the study of metal−metal bonding.[15] Since the molecular isomerism has been observed to be a solid-state effect, this type of analysis is preferentially carried out on solid-state structures. The ED of a crystalline system can be estimated experimentally from accurate X-ray diffraction data,[16] and indeed the X-ray charge density method has been used with success in numerous studies for the past 40 years.[17] In the past decade there have been major advances in the experimental method with the availability of area detectors, intense short wavelength synchrotron radiation and stable helium cooling devices.[18] Apart from experimental charge density analysis we also scrutinize the intermolecular interactions in the crystal structures of the *u*-**1** and *s*-**1** by using the Hirshfeld surface analysis pioneered by Spackman and co-workers.[19]

Experimental Section

Conventional Data. The crystals used in the present study came from the same batch and they were synthesized according to published procedures.[8] Single crystal Mo Kα X-ray diffraction data were collected at 100 K on a Bruker SMART 1K diffractometer equipped with an Oxford Cryosystem liquid nitrogen cooling device located at University of Aarhus, Denmark. A crystal of dimensions $0.20 \times 0.25 \times 0.31$ mm^3 was attached to a glass fiber using Paratone-N oil and attached to a goniometerhead. The data collection consisted of a combination of omega and phi scans with a scan width of 0.3°. Data reduction and structure solution was done with the Bruker SMART suite of programs (SAINT+, SADABS, SHELX).[20] An empirical absorption correction was performed using the highly redundant data. Some hydrogen atoms were located by Fourier synthesis, and the remaining placed on calculated positions. Since the precise solvent content is important, refinement of solvent occupancies was carefully monitored. A fully and two partly occupied solvent sites were refined in the model, but other solvent sites with low occupancy cannot be ruled out. The solvent occupancies were refined for five different data sets collected on three different crystals from the same synthesis batch (see Supporting Information). The total solvent content varies from 2.08 to 2.17 CH_2Cl_2 molecules, being 2.11 for the 100 K data sets used in the ED modeling. The constancy of the solvent content for all the crystals suggests that this value is determined by the crystallization conditions.

The ED was modeled using the Hansen−Coppens multipole model[21] as coded in the XD software package.[22] Only the electron density deformation of the $Co_3(dpa)_4Cl_2$ complex was modeled with multipole functions, whereas the solvent molecules were imported as neutral entities into XD with fixed occupancies obtained from the SHELX program for structural refinement.[15f] The multipole model used $l_{max} = 4$ for Co, $l_{max} = 3$ for C, N and O, and a monopole and a bond directed dipole on H. For the non-hydrogen atoms single Slater-type radial functions were used, whereas the

(13) (a) Pantazis, D. A.; McGrady, J. E. *J. Am. Chem. Soc.* **2006**, *128*, 4128–4135. (b) Pantazis, D. A.; Murillo, C. A.; McGrady, J. E. *Dalton Trans.* **2008**, 608–614.

(14) Bader, R. F. W. *Atoms in Molecules: A Quantum Theory*; Clarendon Press, Oxford, 1990.

(15) (a) Bianchi, R.; Gervasio, G.; Marabello, D. *Acta Crystallogr., Sect. B* **2001**, *57*, 638–645. (b) Bianchi, R.; Gervasio, G.; Marabello, D. *Inorg. Chem.* **2000**, *39*, 2360–2366. (c) Macchi, P.; Proserpio, D. M.; Sironi, A. *J. Am. Chem. Soc.* **1998**, *120*, 13429–13435. (d) Macchi, P.; Garlaschelli, L.; Martinengo, S.; Sironi, A. *J. Am. Chem. Soc.* **1999**, *121*, 10428–10429. (e) Farrugia, L. J.; Mallinson, P. R.; Stewart, B. *Acta Crystallogr., Sect. B* **2003**, *59*, 234–247. (f) Clausen, H. F.; Overgaard, J.; Chen, Y. S.; Iversen, B. B. *J. Am. Chem. Soc.* **2008**, *130*, 7988–7996. (g) Overgaard, J.; Clausen, H. F.; Platts, J. A.; Iversen, B. B. J. *J. Am. Chem. Soc.* **2008**, *130*, 3834–3843.

(16) (a) Coppens, P. *X-ray Charge Densities and Chemical Bonding*; Oxford Science Publications: New York, 1997.

(17) (a) Koritsanszky, T.; Coppens, P. *Chem. Rev.* **2001**, *101*, 1583–1627. (b) Coppens, P.; Larsen, F. K.; Iversen, B. B. *Coord. Chem. Rev.* **2004**, *249*, 179–195.

(18) (a) Koritzansky, T.; Flaig, R.; Zobel, D.; Krane, H.-G.; Morgenroth, W.; Luger, P. *Science* **1998**, *279*, 356–358. (b) Iversen, B. B.; Larsen, F. K.; Pinkerton, A.; Martin, A.; Darovsky, A.; Reynolds, P. A. *Acta Crystallogr., Sect. B* **1999**, *55*, 363–374. (c) Overgaard, J.; Schiøtt, B.; Larsen, F. K.; Iversen, B. B. *Chem.−Eur. J.* **2001**, *7*, 3756–3767. (d) Overgaard, J.; Iversen, B. B.; Palii, S. P.; Timco, G. A.; Gerbeleu, N. V.; Singerean, L.; Larsen, F. K. *Chem.−Eur. J.* **2002**, *8*, 2775–2786. (e) Poulsen, R. D.; Bentien, A.; Chevalier, M.; Iversen, B. B. *J. Am. Chem. Soc.* **2005**, *127*, 9156–9166. (f) Poulsen, R. D.; Jørgensen, M.R. V.; Overgaard, J.; Larsen, F. K.; Morgenroth, W.; Graber, T.; Chen, Y.; Iversen, B. B. *Chem.−Eur. J.* **2007**, *13*, 9775–9790. (g) Morgenroth, W.; Overgaard, J.; Clausen, H. F.; Svendsen, H.; Jørgensen, M. R. V.; Larsen, F. K.; Iversen, B. B. *J. Appl. Crystallogr.* **2008**, *41*, 846–853.

(19) (a) Spackman, M. A.; Byrom, P. G. *Chem. Phys. Lett.* **1997**, *267*, 215–220. (b) Spackman, M. A.; McKinnon, J. J. *CrystEngComm* **2002**, *4*, 378–392. (c) McKinnon, J. J.; Spackman, M. A.; Mitchell, M. S. *Acta Crystallogr., Sect. B* **2004**, *60*, 627–668. (d) McKinnon, J. J.; Jayatilaka, D.; Spackman, M. A. *Chem. Commun.* **2007**, 3814–3816. (e) Spackman, M. A.; McKinnon, J. J.; Jayatilaka, D. *CrystEngComm* **2008**, *10*, 377–388. (f) Spackman, M. A.; Jayatilaka, D. *CrystEng-Comm* **2009**, *11*, 19–32.

(20) Sheldrick, G. S. *Acta Crystallogr., Sect. A* **2008**, *64*, 112–122.

(21) Hansen, N. K.; Coppens, P. *Acta Crystallogr., Sect. A* **1978**, *34*, 909–921.

(22) Koritsanszky, T.; Howard, S. T.; Richter, T.; Macchi, P.; Volkov, A.; Gatti, C.; Mallinson, P. R.; Farrugia, L. J.; Su, Z.; Hansen, N. K. *XD - A Computer Program Package for Multipole Refinement and Topological Analysis of Charge Densities from Diffraction Data*; 2003; http://xd.chem.buffalo.edu.

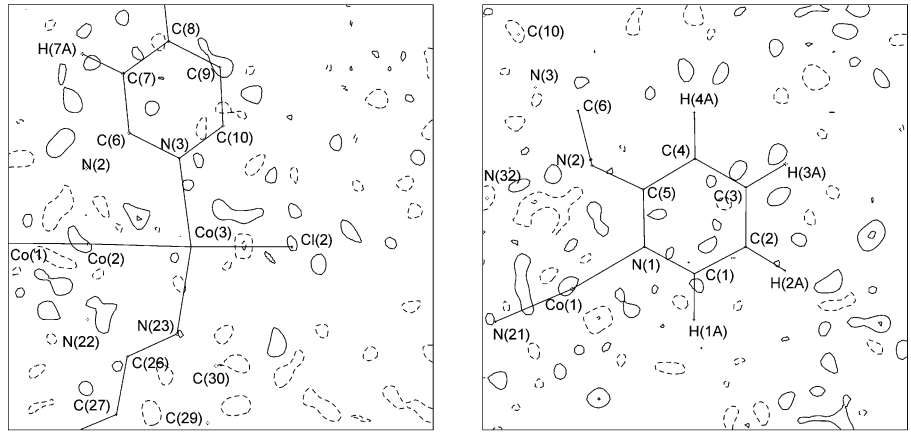

Figure 2. Residual density maps of (a) the N(3)−Co(3)−Cl(2) plane and (b) N(1)−C(2)−C(4) plane calculated using all data. The contour level is 0.1 e Å^{-3} with solid contours being positive and dashed contours being negative. The largest residuals are in the formally neutral solvent molecules with extrema of −0.95 and 1.58 e Å^{-3}.

Table 1. Crystallographic and Experimental Data for $Co_3Cl_2N_{12}C_{40}H_{32}\cdot 2.11CH_2Cl_2$ (*u*-**1**)

formula weight (g mol^{-1})	8838(3)				
space group	tetragonal $I\bar{4}$				
T (K)	20(1)	20(2)	100	150(2)	300(1)
a (Å)	27.067(2)	27.103(1)	27.132(3)	27.247(1)	27.483(1)
b (Å)	27.067(2)	27.103(1)	27.132(3)	27.247(1)	27.483(1)
c (Å)	12.244(2)	12.240(1)	12.201(2)	12.257(1)	12.376(1)
V (Å^3)	8970(1)	8991(1)	8982(1)	9100(1)	9347(1)
λ (Å)	0.643(1)	0.643(1)	0.71073	0.643(1)	0.643(1)
Z	8	8	8	8	8
ρ_{calc} (g cm^{-3})	1.641	1.632	1.634	1.610	1.562
μ (mm^{-1})	1.08	1.08	1.52	1.07	1.04
N_{ref}	140150	216077	133179	173139	59854
N_{unique}	32470	51289	30432	43319	21748
R_{int}	0.0463	0.0676	0.0405	0.0572	0.0387
$(\sin(\theta)/\lambda)_{max}$ (Å^{-1})	0.99	1.24	0.95	1.17	0.88
N_{par}	597	597	850	588	588
N_{obs} (2σ)	27877	37899	13322(3σ)	30883	15797
$R(F)$ (2σ)	0.0468	0.0528	0.0461(3σ)	0.0565	0.0534
$R(F)$	0.0575	0.0736	0.0506	0.0812	0.0812
$R_w(F^2)$	0.1231	0.1317	0.0552	0.1353	0.1403
GoF	1.03	0.95	1.32	0.97	1.01

hydrogen atoms used the SDS scattering factor.[23] Neutral scattering factors were employed for Co.[24] The hydrogen atoms were moved along the bond directions to positions giving bond distances equal to average neutron diffraction values (1.084 Å). Because ED modeling on a molecule with this size and complexity is not straightforward, several multipole models having various degrees of radial flexibility as well as chemical constraints were tested. Divergence was observed with free refinement of all multipole parameters on every atom. Thus, the four dpa groups were constrained to have identical multipole parameters. Additionally, the radial κ' and κ'' parameters were constrained to be identical for each unique atom type. The resulting residual density in selected planes is shown in Figure 2. When separate refinement of κ' and κ'' was carried out on all heavy atoms, the residual was not significantly lowered but lead to unrealistically low values of κ'' for nitrogen and chlorine atoms, a problem often encountered on terminal atoms. Separate radial κ parameters were introduced for the three unique Co atoms, and the final values ($\kappa' = \kappa''$) for all atoms were: κ'(Co(1)) = 0.778(4), κ'(Co(2)) = 0.810(5), κ'(Co(3)) = 0.875(6), κ'(Cl) = 0.894(3), κ'(N) = 0.958(3), κ'(C) = 0.941(3). The Hirshfeld rigid bond test[25] gives a quite high mean Δ_{A-B} value of 18.8 pm^2 with highest values in C−N and C−C bonds within the dpa molecules. Because the topological features of the static electron density discussed below compare well with literature values, and the deformation densities in well-known functional groups show expected features, we nevertheless have confidence in the final multipole model. The enlarged Δ_{A-B} values may be due to the presence of slight disorder caused perhaps by the coexistence of two different spin isomers with slightly different nuclear coordinates. Such slight disorder presumably will be absorbed in the atomic displacement parameters (ADPs) leading to increased Δ_{A-B} values. However, overall the derived static electron density appears to be robust, and the features being discussed are believed to be significant beyond the influence of small disorder features. If the crystal indeed consists of molecules in two different electronic states, the modeled ED represents a weighted average. Experimental and crystallographic details are listed in Table 1.

Initially, we intended to carry out multitemperature experimental ED measurements to allow a mapping of the changes in d-electron populations on the metals with temperature. This may provide firm conclusion about the origin of the structural changes and the

(23) Stewart, R. F.; Davidson, E. R.; Simpson, W. T. *J. Chem. Phys.* **1965**, *42*, 3175–3187.
(24) Clementi, E.; Roetti, C. *At. Nucl. Data Tables* **1974**, *14*, 177.
(25) (a) Harel, M.; Hirshfeld, F. L. *Acta Crystallogr., Sect. B* **1974**, *31*, 162–172. (b) Hirshfeld, F. L. *Acta Crystallogr., Sect. A* **1976**, *32*, 239–244.

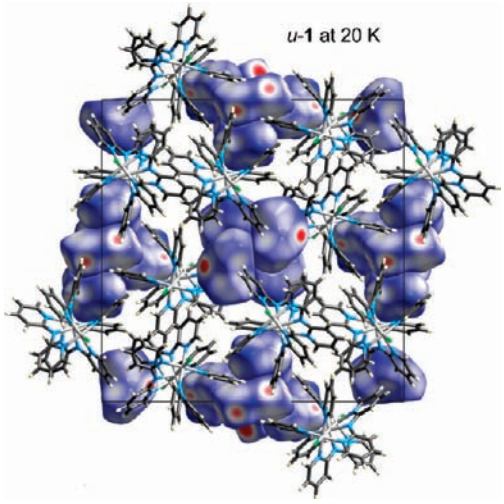

Figure 3. Cell packing diagram for *u*-**1** at 20 K (view down ***c***). Solvent molecules are represented as Hirshfeld surfaces mapped with d_{norm}, and *u*-**1** complex as tube models.

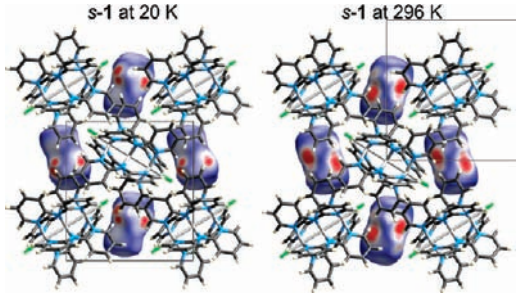

Figure 4. Cell packing diagrams for *s*-**1** at 20 K (view down ***a***) and at 296 K (view down ***c***) showing the nearly identical crystal structures at the two temperatures. Solvent molecules are represented as Hirshfeld surfaces mapped with d_{norm}, and the *s*-**1** complex as tube models.

magnetism in the system. However, in the present study we can only report the ED based on Mo Kα diffraction data collected at 100 K. Several attempts to collect data at other temperatures, including synchrotron microcrystal experiments (see below), did not result in data suitable for charge density modeling, although acceptable spherical atom crystal structure data were attainable at 20 K, 150 K, and 300 K.

Synchrotron Data. Diffraction data were also collected using synchrotron X-ray radiation ($\lambda = 0.643(1)$ Å) at beamline X3A1 at the National Synchrotron Light Source, U.S.A., at 20, 150, and 300 K. The 20 K and the 300 K data were collected during one beam time period, whereas a second 20 K set and the 150 K data were collected during a second beam time period. Since the crystals lose interstitial molecules with time, causing significant crystal degradation, reliable charge density modeling was unsuccessful for these data, even though the very low temperature data would have been expected to provide higher resolution than the conventional 100 K data. The conventional 100 K data were collected shortly after the synthesis. Nevertheless, the spherical atom crystal structures are of good quality and provide a useful comparison with earlier multitemperature studies.[8] For the synchrotron data collections, single crystals were mounted on a few carbon fibers and placed in the cold He stream of a Pinkerton-type cooling device[26] fitted on a Huber-type 512 four-circle diffractometer. The diffracted radiation in the ϕ-scan experiments was detected with a Bruker 6000 CCD detector mounted on the 2θ arm of the diffractometer at a distance of 7.36 cm. The data reduction was performed with the Bruker SAINT package,[27] and data averaging was done with program SORTAV.[28] Further experimental details are given in Table 1.

Results and Discussion

Intermolecular Interactions: *s*-1 vs *u*-1. Crystal engineering, a very active field of chemical crystallography,[29] tries to describe, understand and exploit the multitude of intermolecular interactions that govern the assembly of molecules into crystals. The traditional approach has been to locate those short intermolecular contacts in the crystal that are believed to be important for the crystal assembly. However, this approach may not capture the significance of multiple weaker interactions that in combination can be of great importance, and as molecular size and complexity increase it becomes a daunting task to decipher the numerous intermolecular interactions in a molecular crystal. A novel approach to the problem was recently introduced by Spackman and co-workers based on the Hirshfeld surface of a molecule in a crystal.[19] Molecular Hirshfeld surfaces partition crystal space into smooth, nonoverlapping, molecular volumes, inside which the electron distribution due to a sum of spherical atoms for the chosen molecule exceeds the corresponding sum over the rest of the crystal, and the Hirshfeld surface is defined implicitly where the two contributions are equal. As it depends intimately on the molecular geometry, the location and orientation of neighboring molecules, and the nature (radial extent) of the atoms making close contacts with the molecule in question, the Hirshfeld surface reflects in considerable detail the immediate environment of a molecule in a crystal.

For each point on the surface, two distances are naturally defined: d_e, the distance from the point to the nearest nucleus *external* to the surface, and d_i, the distance to the nearest nucleus *internal* to the surface. Color mapping of these distances on the Hirshfeld surface, as well as a number of properties based on surface curvature, has been explored in some detail.[19] For the present purposes we use the normalized contact distance based on both d_e and d_i, and defined by $d_{norm} = (d_i - r_i^{vdW})/r_i^{vdW} + (d_e - r_e^{vdW})/r_e^{vdW}$, where r_i^{vdW} and r_e^{vdW} are van der Waals radii of the atoms that determine d_e and d_i for each point on the surface.[19d] We map d_{norm} on the Hirshfeld surface with a color range from red (shorter than the sum of van der Waals radii) through white (equal to the sum of radii) to blue (greater than the sum of radii). In this fashion the d_{norm} surface is largely blue, with red spots corresponding to intermolecular contacts shorter than the sum of van der Waals radii. Because of the symmetry between d_e and d_i in the expression for d_{norm}, where two Hirshfeld surfaces touch, both will display a red spot identical in color intensity as well as size and shape, Figure 3. 2D fingerprint plots[19b] are derived from the Hirshfeld surface by plotting the fraction of points on the surface as a function of the pair (d_i, d_e). Each point on the standard 2D graph represents a bin formed by discrete intervals of d_i and d_e (0.01 Å × 0.01 Å), and the points are colored as a function of the fraction of surface points in that bin, with a range from blue (relatively few points) through green (moderate fraction) to red (highest fraction). To date, most fingerprint plots have used the standard range of fractions spanning 0.1% of surface area, but

(26) Hanson, B. L.; Martin, A.; Harp, J. M.; Bunick, C. G.; Parrish, D. A.; Kirschbaum, K.; Bunick, G. J.; Pinkerton, A. A. *J. Appl. Crystallogr.* **1999**, *32*, 814–820.

(27) *SAINT v7.12A*; Bruker AXS Inc.: Madison, WI. 2005.

(28) Blessing, R. H. *J. Appl. Crystallogr.* **1997**, *30*, 421–426, and references therein.

(29) Desiraju, G. R. *Crystal Engineering: The Design of Organic Solids*; Elsevier: Amsterdam, 1989.

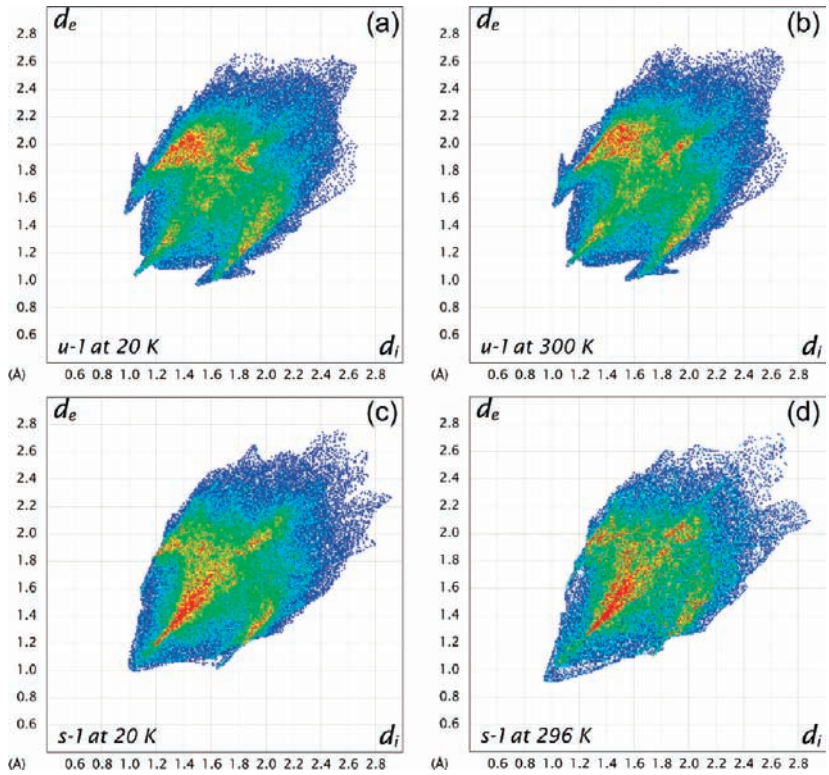

Figure 5. Fingerprint plots for (a) *u*-**1** at 20 K, and (b) 300 K (Table 1), and for (c) *s*-**1** at 20 K (RIBKES05), and (d) 296 K (RIBKES03); CSD refcodes are given in parentheses.

to facilitate more detailed visual comparison between plots, those presented below use an enhanced color scale, spanning a range of 0.033% (i.e., enhanced by a factor of 3).[30]

For the extended metal chain structures there are a number of issues that must be addressed. In particular, we must examine whether the intermolecular interactions in *u*-**1** and *s*-**1** change significantly with temperature to probe whether the crystal environment has a direct bearing on the dramatic changes in magnetism of the crystal, and we also need to investigate the role of solvent molecules in the different structures. For *s*-**1** there is a phase transition at 165 K, where the crystal environment must change, and this makes it difficult to disentangle structural and magnetic effects.[8] Interestingly, it has been noted that *s*-**1** in the low-temperature phase achieves unsymmetrical hydrogen-bonding interactions between the two Cl ends of the molecule due to solvent ordering.[8] Thus, the trimetal chain is believed to be symmetric at low temperature despite the asymmetric crystal environment. On the other hand *u*-**1** maintains the same crystal symmetry from 20 to 300 K, a temperature range in which the molecular magnetic moment changes by a factor of 2.

(30) All results in this section have been obtained with a computer program for calculation and display of Hirshfeld surfaces and 2D fingerprint plots (Wolff, S. K.; Grimwood, D. J.; McKinnon, J. J.; Jayatilaka, D.; Spackman, M. A. *CrystalExplorer2.1.*; University of Western Australia: Crawley, Western Australia, 2007; http://hirshfeldsurface.net/CrystalExplorer). *CrystalExplorer* accepts a structure input file in CIF format and because internal consistency is important when comparing structures, for the generation of Hirshfeld surfaces and all related properties; all bond lengths to hydrogen (or deuterium) atoms are set to typical neutron values (C−H = 1.083 Å, O−H = 0.983 Å, N−H = 1.009 Å; Allen, F. H.; Kennard, O.; Watson, D. G.; Brammer, L.; Orpen, A. G.; Taylor, R. *J. Chem. Soc., Perkin Trans. 2* **1987**, S1−S19). Internuclear separations involving H atoms quoted in this section refer to these standardized proton positions.

Unit cell packing diagrams are depicted in Figure 3 for *u*-**1** at 20 K (the packing is identical to that at 300 K) and in Figure 4 for *s*-**1** at 20 K and at 296 K. In these figures the solvent molecules are represented by Hirshfeld surfaces mapped with d_{norm}, and these diagrams highlight the differing solvent content of the *u*-**1** and *s*-**1** crystal structures, as well as identifying the weak hydrogen-bonding arrangements of the solvent molecules. In the crystal structure of *u*-**1** solvent dichloromethane molecules cluster around two sites of $\bar{4}$ symmetry in space group $I\bar{4}$. The four around (0,0,(1)/(2)) are ordered, fully occupied, and engage in C−H···Cl−Co hydrogen bonds with the complex, and weak C−H···Cl interactions among themselves, while around the site at (0,(1)/(2),(1)/(4)) four solvent molecules are ordered, with an occupancy ∼85%, and another two lie along a two-fold axis, and are disordered with an occupancy ∼50%. These solvent molecules engage in weaker C−H···Cl−Co hydrogen bonds with the complex, and also C−H···Cl interactions with the pyridyl rings of the complex. For *u*-**1** close to 19% of the cell is occupied by solvent (measured by the volumes of the Hirshfeld surfaces of the solvent molecules), and this estimate is independent of temperature. From Figure 4 we see that the packing for *s*-**1** at 20 K is almost identical with that at 296 K, the only substantial difference being the ordering of the solvent dichloromethane molecule. From the figure we can see two equivalent close contacts made by the solvent molecules at 296 K, and the environments of the two Cl ligands at each end of the *s*-**1** complex are identical, while at 20 K only a single contact is evident, and this occurs with only one of the Cl ligands of the complex (this is best seen around the central complex molecule in each packing diagram). For *s*-**1** at 296 K 10% of the cell is occupied by solvent, while at 20 K this drops to 8%, a direct consequence of the solvent ordering.

Table 2. Fingerprint Breakdowns Given as Percentages of Total Area of the Hirshfeld Surface of the Complex

	u-**1** at 20 K	*u*-**1** at 300 K	*s*-**1** at 20 K	*s*-**1** at 296 K
H···H	55.5	56.8	62.6	64.0
H···C/C···H	20.9	19.5	19.3	18.5
H···Cl/Cl···H	17.4	18.0	11.8	11.8
C···C	1.3	1.1	1.7	1.0
C···Cl/Cl···C	3.5	3.3	3.7	3.8

Figure 5 shows fingerprint plots for both *u*-**1** and *s*-**1** at 20 K and at room temperature, based on the present (*u*-**1**) and the previously (*s*-**1**) reported structural refinements. The similarity between the two *u*-**1** plots is striking, and close comparison reveals that they are almost superimposable except for an obvious shortening of distances in the 20 K plot relative to the 298 K plot, which reflects the thermal contraction of the *u*-**1** crystal. The plots for *u*-**1** reveal two obvious intermolecular contacts. The first contact gives the "wings" of the plot at (d_i,d_e) in the range (1, 1.5) to (1.2, 1.8), and these are due to C−H···π interactions. The second conspicuous feature is the spike at lower left, along the plot diagonal, due to two very short H···H contacts: H3···H12 (2.085 Å) and H2···H13 (2.243 Å). There is no evidence of the complexes participating in strong hydrogen bonds, which would be seen as off-diagonal spikes extending down to ∼0.6 Å in either d_i or d_e, although there is evidence of them accepting weak C−H···Cl−Co interactions in the yellow streaks at the bottom right of the plots (especially notable in *s*-**1** at 20 K). Considering the large number of aromatic rings in the complexes the amount of $\pi-\pi$ stacking, typically seen around $(d_i,d_e) \sim (1.8, 1.8)$, is also fairly limited; the packing appears to be influenced more by C−H··· interactions than by π···π stacking. Comparing the fingerprint plots of *s*-**1** at 20 and 296 K, it appears that the room temperature print has a narrower shape and extends to slightly shorter contacts (∼0.9 Å). With the exception of the diffuse area of points at unphysically short d_i or d_e for *s*-**1** at 296 K, which arise from contacts with the disordered solvent molecule and which disappear at 20 K, the fingerprint plot does not obviously reflect the phase transition at 165 K, and the reason for this is evident from Figure 4. In summary, the fingerprint plot for *u*-**1** is characteristic of a polycyclic aromatic hydrocarbon such as anthracene, while the plot for *s*-**1** has more features in common with structures that incorporate packing of alkyl chains (i.e., a large number of nondirectional but relatively close H···H contacts).[19]

Next we compare the intermolecular interactions between *s*-**1** and *u*-**1**. Again the fingerprints effectively expose large differences between crystal packing for the two molecules. Thus, *s*-**1** lacks the wings due to C−H···π interactions as well as the diagonal spike due to specific head-to-head H···H contacts, which are so conspicuous for *u*-**1**. The fingerprint plot reveals that *s*-**1** has few strongly directional contacts, suggesting that the molecule experiences a quite isotropic crystal environment, which is unlikely to force the breaking of the molecular symmetry. The fingerprint plots can be decomposed into contributions from specific atom types,[19d] and this breakdown can be used to provide a measure of the relative importance of various interactions when comparing crystal structures. Table 2 summarizes the data for structures of *u*-**1** and *s*-**1** at 20 K and at room temperature. Comparing the results between 20 K and room temperature, there are no significant differences evident in the breakdowns, reinforcing the fact that the crystal structure of *u*-**1** is unaltered over this temperature range, and the phase change observed for *s*-**1** at 165 K leads to no significant disruption of the crystal packing. Despite the differences noted in appearance of the fingerprint plots, the contribution from interactions of C−H···π type (the sum of C···H and H···C areas, Table 2) does not differ greatly between *u*-**1** and *s*-**1**. On the other hand the different fractions of H···H and H···Cl/Cl···H areas for *u*-**1** compared with *s*-**1** seem highly significant, and a consequence of the greater solvent content of *u*-**1** compared to *s*-**1**; in effect a doubling of the number of solvent molecules results in more contacts between complex and solvent molecules (of H···Cl/Cl···H type) and fewer between complex molecules (of H···H type).

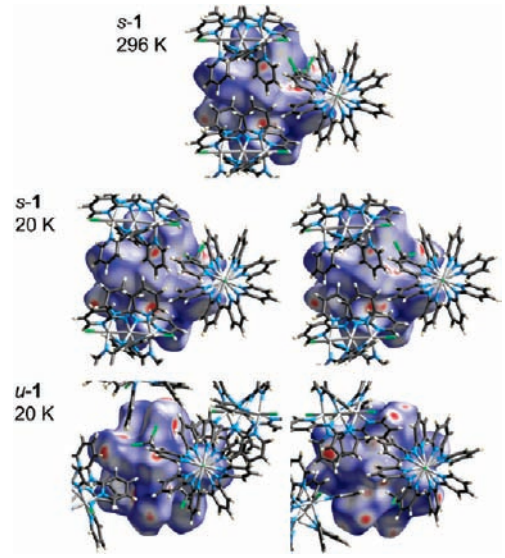

Figure 6. Hirshfeld surfaces mapped with d_{norm}, showing the nearest neighbor environment around each Cl ligand of the $Co_3(dpa)_2Cl_2$ complex. In all cases the view is along the Cl−Co−Co−Co-Cl axis of the complex within the surface, and only molecules with an atom within 5 Å of the Cl ligand are shown. For *u*-**1** and *s*-**1** at 20 K the left view shows the environment around Cl(2) and the right view that around Cl(1); for *s*-**1** at 296 K both Cl atoms have identical environments and only one end of the molecule is shown.

The key issue in this analysis of intermolecular interactions for these crystal structures is the question of asymmetry of the intermolecular contacts in *u*-**1** versus symmetry of the same in *s*-**1**. This is indeed the case, and it is revealed in striking fashion when examining d_{norm} plotted on the Hirshfeld surfaces, Figure 6, which views the two ends of each complex molecule along the Cl−Co−Co−Co−Cl axis. These figures contain a great amount of information, and they merit a detailed discussion. As already noted the red spots on these d_{norm} surfaces highlight intermolecular contacts closer than the sum of van der Waals radii, and the patterns made by them can readily identify similarities and differences between ends of these complexes. We focus on *s*-**1** first, for which it is evident from the red spots on the surfaces that the two ends of the complex at 20 K are much the same and, moreover, both are little different from the environment found at 296 K; the differences are due almost entirely to the ordering of the solvent molecule. The disordered solvent is evident at the top right of the surface at 296 K, and it is the disorder that guarantees that both ends of the *s*-**1** complex are involved in identical interactions with the solvent. Ordering of the solvent affects the two ends differently, and at 20 K it is clear that Cl(1) in *s*-**1** accepts a weak C−H···Cl−M hydrogen bond (H···Cl = 2.66 Å, C−H···Cl angle 174.5°), while at the other end the closest solvent H atom is 3.89 Å

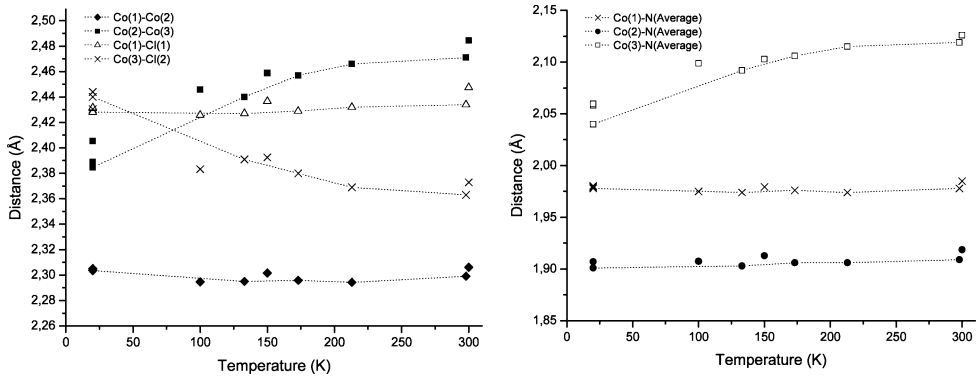

Figure 7. Selected bond lengths as a function of temperature. The lines correspond to literature values taken from ref 8.

from the Cl(2) ligand. Several other relatively close contacts to the ligand Cl atoms are made by pyridyl H atoms, the most obvious being to the H atom directly above the Cl ligand in each figure. Ordering of the solvent also results in a subtle rearrangement of these pyridyl groups around the terminal Cl atoms, and as a result this contact distance, which is 3.29 Å at 296 K, shortens at 20 K to 3.14 Å at Cl(1), which is closest to the ordered solvent molecule, and 3.01 Å at Cl(2), which is more distant from the solvent molecule. Thus, the absence of a bulky dichloromethane molecule close to a terminal Cl atom of the complex enables the pyridyl ring to approach much closer to the Cl atom.

In contrast to *s*-**1**, the two ends of the *u*-**1** complex are quite clearly different from one another, as seen in the arrangement of close contacts on the d_{norm} surface, as well as the disposition of neighboring molecules. The Cl(2) end participates in a relatively strong C−H···Cl−M hydrogen bond with a solvent molecule (occupancy = 1.0) at top center of the figure (H···Cl = 2.60 Å, C−H···Cl angle 144.8°), and a much longer contact with a different solvent molecule (occupancy = 0.828 at 20 K) at lower right of the figure (H···Cl = 3.08 Å, C−H···Cl angle 175.2°). In addition there is a close C(pyridyl)−H···Cl−M contact of 3.02 Å. In contrast the Cl(1) end of *u*-**1** participates in a single weak hydrogen bond to a solvent molecule (H···Cl = 2.77 Å, C−H···Cl angle 140.3°), but a much closer C(pyridyl)−H···Cl−M contact of 2.85 Å. The view of the *u*-**1** Hirshfeld surface toward Cl(2) in Figure 6 also shows three C−H···π interactions as red spots in the center of circular depressions on the surface, each associated with close approach of a pyridyl H atom.

The present Hirshfeld surface analysis documents that the solvent dichloromethane molecules strongly affect the crystal field experienced by the linear tricobalt unit, and the different environments of the terminal Cl atoms of the complex can be succinctly described in terms of the presence or absence of solvent, and even its relative proximity to the Cl atoms. The intermolecular contacts are shorter, more directional and more unsymmetrical in *u*-**1** than in *s*-**1**, but whether this is the driving force for the molecular isomerism, or a consequence of it, is impossible to conclude, although it seems likely that the interplay among interactions involving the Cl ligand atoms and the neighboring solvent or complex molecules stabilizes the *u*-**1** isomer. An unambiguous answer will require similar detailed analyses of the intermolecular interactions in a large number of linear chain crystal structures, and this is the topic of an ongoing study.

Structure and Electron Density. The temperature dependencies of selected bond lengths in *u*-**1** are shown in Figure 7 using the present as well as published literature values.[8] All bond distances to Co(3) show a dramatic change with temperature, whereas other bond lengths are essentially constant. Since the structural changes correlate strongly with the observed changes in the magnetic properties, it appears that the magnetism is related to the Co(3) atom. The metal chain has been described as a Co_2^{2+} diamagnetic dimer involving Co(1) and Co(2), whereas Co(3) behaves as an isolated magnetic Co^{2+} ion.[12] The correspondence is excellent between the bond lengths obtained for the three different crystals in the present study and the literature data except for bonds involving the Co(3) atom. The fact that it is only the bond lengths to a specific atom that deviate strongly between different crystal structures suggests that the differences are real and not due to systematic errors. The main difference between the present study and the literature data[8] is the slightly different solvent content. This slight difference in solvent content only has a significant effect on the structural behavior of the magnetic Co(3) atom. This indicates that even the magnetism can not be treated as an isolated molecular property unaffected by the supermolecular entity.

Most known linear chain metal complexes are symmetric,[9b] but it should be noted that sometimes small disorder features can be absorbed in the ADPs giving enlarged ADP values along the chain direction. Indeed, improved structural modeling later led to a revision of a number of structures, which are now considered unsymmetrical.[11] Disorder components in the ADPs are best revealed by calculation of ΔU values along the bond direction, and such values have been used in many studies to discuss dynamic processes in crystals.[31] The ΔU values for the Co−Co contacts in the present complex (Figure 8) reveal a likely presence of disorder involving Co(3), while the other parts of the molecule *u*-**1** behave more like a rigid body. Figure 8 shows also that the ΔU values for bonds to Co atoms are relatively unaffected by temperature changes, while it is clear that the dpa molecules appear less rigid with increasing temperature (Figure 8a). These combined structural observations may be explained by the existence of two different spin states within the examined crystal at all temperatures, and it appears that the effects of this are limited to the coordination sphere of Co(3).

As mentioned previously, the chemical bonding in linear unsymmetrical metal-chain complexes such as **1** has been

(31) (a) Chandrasekhar, K.; Bürgi, H. B. *Acta Crystallogr., Sect B* **1984**, 387–397. (b) Stebler, M.; Bürgi, H. B. *J. Am. Chem. Soc.* **1987**, *109*, 1395–1401. (c) Wilson, C.; Iversen, B. B.; Overgaard, J.; Larsen, F. K.; Wu, G.; Palii, S. P.; Timco, G. A.; Gerbeleu, N. V. *J. Am. Chem. Soc.* **2000**, *122*, 11370–11379.

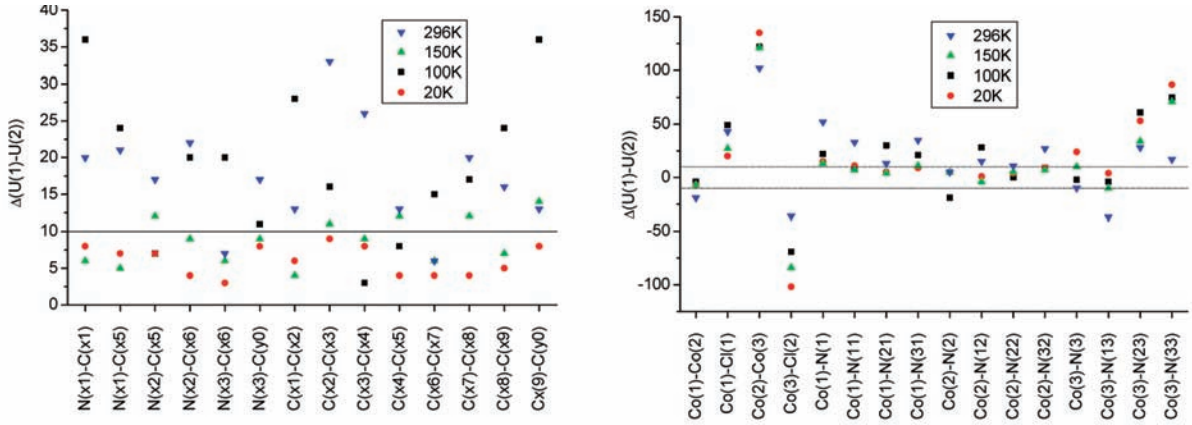

Figure 8. Temperature dependencies of the differences of mean square displacement amplitudes for (a) the average of the bonds in the dpa molecules and (b) the bonds to Co atoms.

described based on MO theory.[12,13] This type of modeling suggests the existence of a single bond between Co(1) and Co(2), but no bonding interaction between Co(2) and Co(3). A difficulty, however, is that MO theory offers no precise definition of chemical bonding.[32] Single bonds in *u*-**1** have been assumed at Co−Co separations from 2.29−2.31 Å, whereas the 3c−3e$^-$ bonds in *s*-**1** have been considered between 2.31 Å and 2.35 Å. Nonbonded Co−Co contacts have been assigned between 2.37 Å and 2.47 Å.[9c] The $Ni_3(dpa)_4Cl_2\cdot 2CH_2Cl_2$ system is symmetrical, but isomorphous to *u*-**1** in the solid state with an almost identical unit cell.[33] MO theory suggested the absence of Ni−Ni bonding for a metal separation of 2.43 Å. The lack of metal−metal bonding is believed to inhibit the Ni system from acting as a molecular wire for Ni_3^{2+} compounds.[33] For symmetrical $Cr_3(depa)_4Cl_2\cdot 0.5$hexane the presumed 3c−3e$^-$ Cr−Cr bond is 2.38 Å.[11] With such similarities in internuclear distances for a range of different metal atoms, it is inherently difficult to differentiate between bonding and nonbonding on the basis of bond lengths alone. Large differences in formal bond orders (qualitative MO theory) may reflect quite small changes both in the metal−metal internuclear distances and in the values of more sophisticated bond order indices.[34] This similarity holds true also for cases which would be classified as bonded or not bonded by MO theory.[34]

The chemical bonding in *u*-**1** can be examined using the charge density derived from X-ray diffraction. Static deformation density maps as well as Laplacian maps are shown in Figure 9 for selected planes, while topological properties calculated at the bond critical points (bcp) are listed in Table 3. Additional planes for the ligands have been deposited in the Supporting Information. For the four constrained dpa moieties the slight differences in bond lengths and angles contribute to differences in topology (see Supporting Information). Starting with the terminal ligands it is clear from Figure 9 that there are substantial differences between the two ends of the trinuclear complex (*u*-**1**) as the two chlorine atoms seems to interact differently with the Co atoms. This is perhaps better illustrated in the plots of the Laplacian isosurface around the Cl atoms as shown in Figure 10. These show a clear sp^3-like distribution of lone-pairs (lp) near Cl(2) with the smallest Co(3)−Cl(2)−lp3 angle of 38° (Figure 10b),

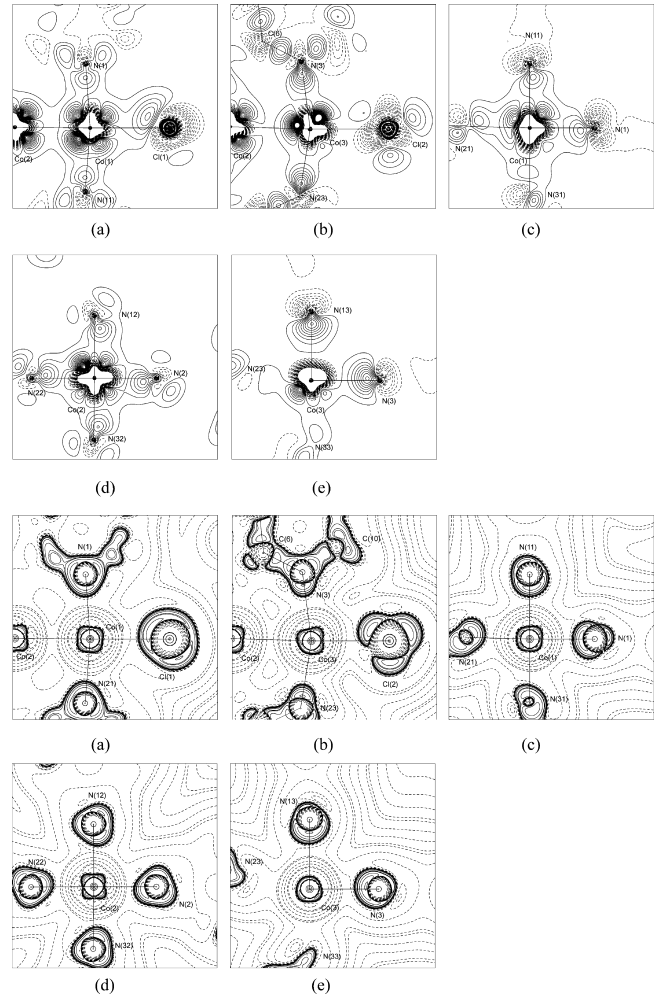

Figure 9. Static deformation (top) and Laplacian (bottom) maps in (a) the N(1)−Co(1)−Cl(1) plane, (b) the N(3)−Co(3)−Cl(2) plane, (c) the N(1)−Co(1)−N(11) plane, (d) the N(2)−Co(2)−N(12) plane, and (e) the N(3)−Co(3)−N(13) plane. The contour level is 0.1 e Å^{-3} for the deformation maps, with solid contours being positive and dashed contours negative. For the Laplacian maps the contour levels are $2^x\cdot 10^y$ e Å^{-5} (x = 0, 1, 2, 3 and y = −2, −1, 0, 1, 2, 3) for the dashed positive contours and for the solid negative contours, respectively.

while the distribution around Cl(1) is better described as sp^2-like (Figure 10a). Here, there are two lp's significantly more prominent

(32) Bader, R. F. W. *Monatsh. Chem.* **2005**, *136*, 819–854.
(33) Aduldecha, S.; Hathaway, B. *J. Chem. Soc., Dalton Trans.* **1991**, 993–998. (a) Clerac, R.; Cotton, F. A.; Dunbar, K. R.; Murillo, C. A.; Pascual, I.; Wang, X. P. *Inorg. Chem.* **1999**, *38*, 2655–2657.
(34) Gatti, C.; Lasi, D. *Faraday Discuss.* **2007**, *135*, 55–78.

Table 3. Selected Topological Measures at the Metal−ligand Bond Critical Points; d_{ij} (Å) Is the Internuclear Distance, DU Is the Difference in ADP along the Bond Direction (pm^2), r_{ij} (Å) Is the Sum of Distances between the Critical Point and the Atomic Attractors, d_1 the Distance (Å) from the First Atom to the Critical Point, ρ is the Electron Density (e Å^{-3}), and $\nabla^2\rho$ the Laplacian (e Å^{-5}); *G*, *V* and *H* Are the Kinetic Energy Density, the Potential Energy Density, and the Total Energy Density, Respectively (hartree Å^{-3})[38]

bond	d_{ij}	DU	r_{ij}	d_1	ρ	$\nabla^2\rho$	*G*	*V*	*H*	G/ρ
Co(1)−Co(2)	2.2946(8)	−4	2.297	1.168	0.32(1)	5.22(1)	0.37	−0.37	0.00	1.13(3)
Co(2)−Co(3)	2.4459(10)	122	2.446	1.219	0.20(1)	3.43(1)	0.21	−0.19	0.03	1.09(5)
Co(1)−Cl(1)	2.4257(9)	49	2.433	1.094	0.47(1)	5.49(2)	0.49	−0.59	−0.10	1.03(4)
Co(3)−Cl(2)	2.3832(11)	−69	2.406	1.101	0.32(1)	3.65(2)	0.29	−0.33	−0.04	0.91(11)
Co(1)−N(1)	1.979(3)	22	1.987	0.981	0.66(2)	9.57(3)	0.85	−1.03	−0.18	1.29(4)
Co(1)−N(11)	1.971(3)	8	1.973	0.982	0.70(1)	10.03(3)	0.91	−1.12	−0.21	1.30(2)
Co(1)−N(21)	1.970(3)	30	1.971	1.009	0.77(1)	11.12(2)	1.03	−1.29	−0.26	1.35(2)
Co(1)−N(31)	1.980(3)	21	1.987	0.968	0.64(1)	9.52(3)	0.82	−0.98	−0.16	1.29(3)
Co(2)−N(2)	1.904(3)	−19	1.933	0.925	0.69(2)	11.46(4)	0.97	−1.14	−0.17	1.40(4)
Co(2)−N(12)	1.908(3)	28	1.912	0.965	0.80(1)	12.89(3)	1.16	−1.42	−0.26	1.44(2)
Co(2)−N(22)	1.916(3)	0	1.933	0.943	0.73(2)	11.75(4)	1.02	−1.22	−0.20	1.40(3)
Co(2)−N(32)	1.902(3)	9	1.907	0.920	0.72(2)	12.61(4)	1.06	−1.23	−0.18	1.46(3)
Co(3)−N(3)	2.105(3)	−2	2.106	1.008	0.49(1)	7.48(4)	0.59	−0.66	−0.07	1.21(5)
Co(3)−N(13)	2.118(3)	−4	2.119	1.021	0.49(1)	7.55(4)	0.60	−0.67	−0.07	1.22(3)
Co(3)−N(23)	2.082(3)	61	2.083	1.009	0.54(1)	8.27(4)	0.67	−0.76	−0.09	1.25(3)
Co(3)−N(33)	2.090(3)	75	2.092	1.023	0.55(1)	8.65(4)	0.70	−0.79	−0.09	1.28(2)

than a third, and the former two are inclined toward Co(1) with approximately equal angles of 55−60°.

The Co(1)−Cl(1) bond is longer than the Co(3)−Cl(2) bond. It has been suggested that the weaker Co(3)−N bonds relatively to Co(1)−N are balanced by a stronger Co(3)−Cl(2) bonds relative to Co(1)−Cl(1).[8] Surprisingly, examination of the topological features at the Co−Cl bcps actually suggests that the longer Co(1)−Cl(1) bond is more covalent than the shorter Co(3)−Cl(2) bond: the value of ρ_{bcp} is 0.47(1) e Å^{-3} in Co(1)−Cl(1) but only 0.32(1) e Å^{-3} in Co(3)−Cl(2). Furthermore, the energy densities confirm this picture of the Co−Cl bonding.[35] However, prudent interpretation is advised since the spin-state disorder probably influences the exact values of the second derivatives of the density. Overall, the topological analysis confirms the expectation that the Co(3)−ligand interactions are more ionic than the Co(1)−ligand interactions, but one cannot on this basis conclude which bond is the strongest in energy terms.[36] In line with the Co−Cl interactions, the Co(1)−N(1) interaction is different from the Co(3)−N(3) interaction. In the pyridine ring there are larger covalent deformation features toward the carbon atoms for N(3) than for N(1). The other pyridine bonds show expected features such as single deformation peaks, and this confirms the reliability of the derived density. The density in the lone pair in the N−Co direction is significantly larger on N(3) than on N(1).

Turning the attention to the Co atoms, the topological analysis contradicts the MO model with a Co_2^{2+} dimer and a separate Co^{2+} ion as bcps are found for both Co(1)−Co(2) and Co(2)−Co(3). As expected, the shorter Co(1)−Co(2) interaction exhibits values suggesting a stronger bond, such as higher ρ_{bcp}, higher $\nabla^2\rho_{bcp}$, and a higher $(G/\rho)_{bcp}$. However, the observation of a Co(2)−Co(3) bcp shows the inherent danger of simple bonding models, in which Co(1)−Co(2) is separated out as a dimer having little interaction with an isolated Co_3^{2+} unit. On the other hand, the topological charges found by integration over the atomic basins (see Table 4) confirm that Co(3) (+1.36) is more ionic than Co(1) (+0.50) and Co(2) (+0.77). The κ parameter is significantly larger for Co(3) (0.875(6)) than for Co(1) (0.778(4)) and Co(2) (0.810(5)), suggesting that the increased ionic character of Co(3) leads to a more contracted electron density. Nevertheless, the chemical interactions appear to be more complex than in the simple ($(Co_2)^{2+}$, Co^{2+}) picture, and interpretation of the spin isomerism as being confined to Co(3) may be a too crude an approximation.

The electron deformation maps shown above in Figure 9 indicate that all metal atoms are distinctly different. The deformation features are clearest on Co(1) and Co(2), where the Laplacian shows strong nonspherical features in the *xy*, *xz*, and *yz* planes (*z* axis along the metal chain, *x* and *y* toward the nitrogen atoms) corresponding to preferred occupancy of the t_{2g} orbitals. The (*xz*, *yz*) features are relatively smaller for the Co(3) atom, corroborating the more ionic character of the Co(3)−Cl(2) interaction. In fact, the deformation around Co(3) is rather unusual, as the 3D Laplacian isosurfaces show (Figure

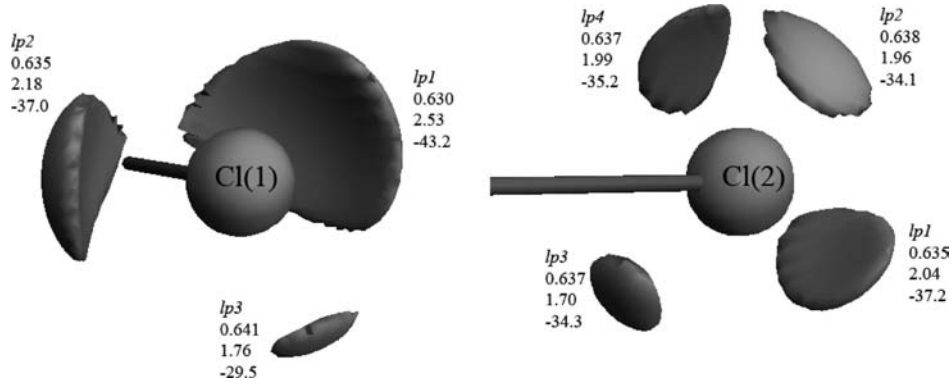

Figure 10. Laplacian isosurfaces around the Cl atoms shown at a value of $\nabla^2\rho = -28$ e Å^{-5}. The average lp−Cl−lp angles are 114(4) and 109(9)° for Cl(1) and Cl(2), respectively. For Cl(1) the Co−lp−Cl angles are 112 and 102°, respectively. For each lp, the three lines of text give (1) the distance to the Cl atom in Å, (2) the value of ρ in e Å^{-3} and (3) the value of $\nabla^2\rho$ in e Å^{-5}.

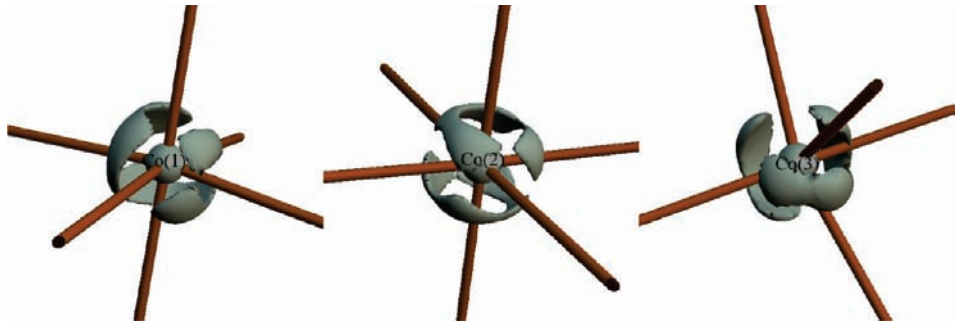

Figure 11. Laplacian isosurfaces of (−1000 e Å^{-5}) around the Co atoms. Properties of the density at the VSCC are shown in the Supporting Information.

Table 4. Atomic Charges, Volumes and Dipole Moments[a]

atom	charge (e)	volume (Å^3)	dipole moment (D)
Co(1)	+0.50	63.0	0.29
Co(2)	+0.77	59.1	0.38
Co(3)	+1.36	65.7	0.25
<N(1*x*)>	−1.37	83.2	0.42
<N(2*x*)>	−1.26	70.9	0.18
<N(3*x*)>	−1.50	86.9	0.48
Cl(1)	−1.61	213.7	1.47
Cl(2)	−0.55	226.4	1.31

[a] For the nitrogen atoms average values are given for the four dpa units.

11). Both Co(1) and Co(2) exhibit the usual eight maxima in the Laplacian corresponding to VSCCs in a cuboid disposition[38] (although not all eight maxima can be clearly distinguished for Co(1)). On the other hand, the distribution around Co(3) is best described as six maxima (three pairs) located in an octahedral fashion around Co(3). As we are not certain whether we observe a true stationary state, this could result from a mixture of two spin states. The analysis of ADPs clearly indicated that there is subtle structural disorder in the Co(3) part of the molecule, which could originate from a mixture of two spin states. On the other hand Co(2), and also Co(1) to a large extent, show expected electronic features, and thus the current picture supports that Co(3) is the atom primarily responsible for the spin changes.

In Figure 12 we show the atomic surfaces of the Co atoms determined from the zero flux boundary condition, and Table 4 lists the atomic charges determined from the basins. As expected from the octahedral coordination the Co atoms are cube shaped, and the twist induced by the dpa unit along the chain axis is clearly seen as a rotation of the cubes with respect to each other along the metal chain. An important point is the substantial difference in atomic charge between Co(1) and Co(2) on one side, and Co(3) on the other, with q(Co(3)) about the size of q(Co(1)) + q(Co(2)). This difference is surprisingly not mirrored in the atomic volumes. The metal−ligand bond critical points are located at a fairly constant distance to the metals, whereas there are differences in the atomic volumes of the coordinating

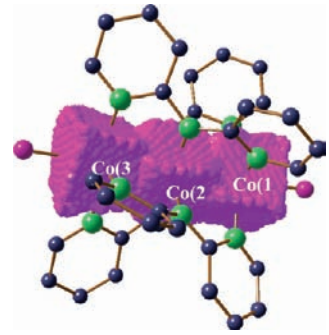

Figure 12. Metal atom zero flux surfaces.

Table 5. Experimental 3d-Orbital Populations for the Cobalt Atoms Derived from the Refined Multipole Parameters[a]

orbital	Co(1)	Co(2)	Co(3)	high-spin Co^{2+}
axis	x_{N1}	x_{N2}	x_{N3}	
axis	y_{N11}	y_{N12}	y_{N13}	
d_{z^2}	1.48(11) 18%	1.11(11) 14%	1.24(15) 17%	14%
$d_{x^2-y^2}$	1.10(11) 13%	0.79(11) 10%	1.18(15) 16%	14%
d_{xz}	2.23(11) 26%	2.05(11) 25%	1.75(15) 23%	21%
d_{yz}	1.91(11) 23%	2.14(11) 26%	1.93(15) 26%	21%
d_{xy}	1.72(11) 20%	2.05(11) 25%	1.38(15) 18%	21%
total	8.44	8.14	7.48	7

[a] The first entry is electron population with estimated standard deviation given in parentheses, and the second entry is the relative population in %.

nitrogen atoms. The atomic charges show a clear difference between the two chlorine atoms with q(Cl(1)) = −1.61 and q(Cl(2)) = −0.55, but the value of Cl(1) appears too high to be fully trusted. It would be of considerable interest to have the experimentally determined topology validated by high-level theoretical calculation.

In Table 5 the experimental d orbital populations derived from the multipole parameters are listed.[39] They reflect the observed density features, where Co(2) shows a tetragonal distortion of the octahedral coordination. Thus, the d_{xy}, d_{xz}, d_{yx} values are large, whereas the destabilized e_g orbitals, $d_{x^2-y^2}$ and d_{z^2}, have smaller occupancies. The absolute values of the d orbital populations derived from the refined multipole parameters are influenced by the monopole values, and therefore also the overall scale of the electron density. This in turn can be affected for example by missing solvent not being modeled. It is therefore preferable to use the relative occupancy of the orbitals to describe the electron deformation features. Comparing Co(1) and Co(2), the value of d_{z^2} is larger on Co(1) while d_{xy} is smaller, which may be explained by the interaction between Co(1) and Cl(1) involving the d_{z^2} orbital on Co(1). On Co(1) there is a

(35) Gibbs, G. V.; Spackman, M. A.; Jayatilaka, D.; Rosso, K. M.; Cox, D. F. *J. Phys. Chem. A* **2006**, *110*, 12259–12266.
(36) Macchi, P.; Schultz, A. J.; Larsen, F. K.; Iversen, B. B. *J. Phys. Chem. A* **2001**, *105*, 9231–9242.
(37) Abramov, Yu A. *Acta Crystallogr., Sect. A* **1997**, *53*, 264–272.
(38) See for instance: (a) Bianchi, R.; Gatti, C.; Adovasio, V.; Nardelli, M. *Acta Crystallogr., Sect. B.* **1996**, *52*, 471–478. (b) Farrugia, L. J.; Mallinson, P.; Stewart, B. *Acta Crystallogr. Sect. B* **2003**, *59*, 234–247.
(39) Holladay, A.; Leung, P.; Coppens, P. *Acta Crystallogr., Sect. A* **1983**, *39*, 377–387.

slight difference between the d_{xz} and d_{yz} values, an asymmetry which originates in the Co(1)−Cl(1) interaction since the basal plane d_{xy} interactions are identical for the four Co−N bonds. For Co(3) the d_{xy} value is significantly decreased, and the $d_{x^2-y^2}$ is significantly increased. In an octahedral field we would expect the d_{xy} orbital to be the lowest in energy, and one may speculate that the spin transition on Co(3) is from d_{xy} to $d_{x^2-y^2}$. Indeed theoretical calculations have shown that a variable $d_{x^2-y^2}$ orbital population with temperature can explain the observed bond length changes around Co(3).[13] Overall, the orbital populations corroborate that Co(3) is clearly different from Co(1) and Co(2).

Conclusions

Hirshfeld surface analysis of intermolecular interactions in *s*-**1** and *u*-**1** has established large differences between the two solvates. In the symmetric system *s*-**1** the two axial termini of the molecule have very similar intermolecular interactions, whereas in *u*-**1** the two ends are very different. It is, however, difficult to judge whether the symmetry of the intermolecular interactions is the origin or an effect of the molecular isomerism. Charge density analysis of *u*-**1** reveals not only that the qualitative picture of a $(Co_2)^{2+}$ dimer and an isolated Co^{2+} ion has some validity but also that the chemical bonding in the molecule is complex. As an example, clear bond critical points are located for both Co−Co interactions. Comparison of new multitemperature structural data with previous measurements on crystals with slightly different solvent content shows that only bonds to the Co(3) atom are affected by the solvent content. Thus, a complete understanding of the bond length changes with temperature cannot be obtained from gas-phase theoretical calculations. Determination of the charge density from the 100 K X-ray data is highly challenging since this acentric crystal probably contains contributions from two spin states as well as disordered solvent molecules. The former explains the unusually large difference ADPs obtained for bonds involving Co(3). Topological analysis gives atomic charges of $Co(1)^{+0.50}$, $Co(2)^{+0.77}$, and $Co(3)^{+1.36}$, and in general the metal−ligand interactions are more ionic for Co(3) than for Co(1) and Co(2). The Co(3) atom has a relatively low occupancy in the d_{xy} orbital and a relatively high occupancy in $d_{x^2-y^2}$ orbital, suggesting that these orbitals are significantly involved in the spin crossover process.

Acknowledgment. We thank Dr. Xiaoping Wang for providing the crystals. We gratefully acknowledge the beam time obtained at beamline X3A1, the National Synchrotron Light Source, Brookhaven National Laboratory, U.S.A. The SUNY X3 beamline at NSLS was supported by the Division of Basic Energy Sciences of the US Department of Energy (DEFG0286ER45231). The work was supported by the DANSCATT center under the Danish Research Councils. MAS acknowledges support from the Australian Research Council. Support by Texas A&M University (TAMU) and the Welch Foundation is also gratefully acknowledged.

Supporting Information Available: Crystallographic information files (CIF) for all measured data (including multipole coefficients for the 100 K data), static deformation and Laplacian maps for two representative planes of the dpa units, refined solvent occupancies for the three crystals, topological properties at the bcps of the ligands, topological properties of maxima in the VSCC of the Co atoms, selected atomic properties, and plots of ρ and $\nabla^2\rho$. This material is available free of charge via the Internet at http://pubs.acs.org.

JA8091032